RESEARCH PAPER

Determination of the poroelasticity of shale

Shuqi Ma[1,2] · Marte Gutierrez[2]

Abstract

Shales play important roles in various civil, energy and environmental engineering applications. Shales are categorized as poroelastic materials due to their tight and very stiff structure, and reliable poroelastic properties are required when dealing with shales. This paper presents simple procedures to determine the poroelastic properties of rocks using oedometer and triaxial consolidation tests. The procedures, which avoid the difficulty to perform determination of the unjacketed bulk modulus of the rock minerals, are demonstrated on a North Sea shale. The experimentally obtained Biot coefficient α and the drained bulk modulus K of the shale range from 0.95 to 0.99, and from 0.17 to 2.00 GPa, respectively. The Biot coefficient α and the drained bulk modulus K values determined from the oedometer and triaxial tests are compared and show good agreement and consistency between the two test procedures. The Skempton's coefficient B-value of the triaxial samples was also experimentally measured prior to the triaxial consolidation tests. The theoretically predicted B-value varies from 0.81 to 0.96 which is, on the average, only about 10% higher than the experimentally obtained B-value which range from 0.80 to 0.85.

Keywords Biot coefficient · Biot's theory · Bulk modulus · Oedometer test · Poroelasticity · Shale · Skempton's B coefficient · Triaxial consolidation test

1 Introduction

Shales are important rock materials which have been encountered in various civil, energy and environmental engineering applications. They constitute the most common cap rock for hydrocarbon reservoirs and potential CO_2 geological storage reservoirs [14, 22]. They are used as geological barriers for the storage of nuclear waste because of their low hydraulic permeability [28, 54]. Shale gas and oil are also typical low-permeability unconventional energy resources [25, 59]. Despite very low permeability, shales in situ often contain high fluid content and can be fully saturated. The presence of fluid in the pores of shales affect their elastic properties. Due to their tight structure

and often very low porosity, the stiffness of a shale matrix can become comparable to the stiffness of its constituent solid mineral grains [7, 28]. Thus, the deformation of fluid saturated shales must also account for deformability of the solid grains due to pore pressure changes [7, 28].

The earliest theory to approach the influence of pore fluid on the deformation of geomaterials was originally developed by Terzaghi [52, 53] for the one-dimensional consolidation of soils. In Terzaghi's consolidation theory, both the pore fluid and the solid particles are considered incompressible, i.e., the compressibility of both the soil and fluid constituents are assumed to be zero. In other words, the bulk modulus of the soil and the fluid are assumed to be infinite. This means that the volume change of soils can only occur due to the change in the volume of the pores. In case the pores are fully saturated with fluids, the change in the volume of fluid becomes equal to the change in the pore and total volume.

The assumption of incompressible solid grains is only an approximation. In the case of soils, this approximation is true because the soil matrix is comparatively much more compressible than the solid grains. The assumption of incompressible solid grain in a compressible matrix is also

✉ Shuqi Ma
shuqima.ma@gmail.com

1 Key Laboratory of Transportation Tunnel Engineering, Ministry of Education, Southwest Jiaotong University, Chengdu 610031, China

2 Civil and Environmental Engineering, Colorado School of Mines, Golden, CO, USA

the basis for Terzaghi's effective stress law [53] which states that: (1) the mechanical response of soils is controlled by effective stresses, and (2) effective stresses are the differences between the total stresses and the pore pressure.

Biot [8] extended Terzaghi's consolidation theory and effective stress law to remove the assumptions of incompressible solid grains and fluids as well as the assumption of one-dimensional consolidation. Biot's modification of the effective stress law requires the Biot coefficient α in the calculation of effective stress σ'_{ij} acting on the grains of shale using the following equation [9].

$$\sigma'_{ij} = \sigma_{ij} - \alpha \delta_{ij} u \qquad (1)$$

where σ_{ij} is total stress tensor, u is the pore pressure and δ_{ij} is the Kronecker delta which gives $\delta_{ij} = 1$ for $i = j$ and $\delta_{ij} = 0$ for $i \neq j$.

Parameters such as the Biot coefficient α and the Skempton's pore pressure coefficient B [49] in the Biot's linear poroelasticity theory can allow the transformations between the drained constants K and v and their undrained counterparts [57]. The Biot coefficient α and the Skempton's coefficient B are essential when exploring and evaluating geo-reservoirs [26, 29], assessing seismic velocities of fluid-filled porous material from dry values [27], and computing the storage coefficient of reservoirs [6]. For elastic fluid saturated porous materials, Biot's work has come to be referred to as poroelasticity theory. At the same time, Biot extended Terzaghi's one-dimensional theory to three-dimensions.

Since its development, Biot's linear theory was reformulated by Verruijt [55] in a specialized version which is suitable for problems in soil mechanics. Rice and Cleary [45] reformulated Biot's linear theory by linking the poroelastic parameters to well-understood concepts in soil and rock mechanics. They presented the equations of consolidation under drained and undrained conditions. Zienkiewicz et al. [60] and Prevost [42, 43] extended Biot's theory to nonlinear constitutive equations. Coussy [21] generalized Biot's theory to include nonlinear material behavior and large deformations using the thermodynamics approach. Gutierrez and Lewis [26] showed the importance of Biot's theory in the coupled fluid flow and geomechanical modeling of subsidence in deformable hydrocarbon reservoirs.

Analysis of the coupled hydro-mechanical response of shales is normally based on Biot's theory. Shales are poroelastic materials in the strictest sense of poroelasticity theory, and a deeper understanding of their poroelastic properties is required when dealing with shales. Determination of the poroelastic properties of rocks often use the so-called unjacketed consolidation test to obtain the bulk modulus of the rock minerals. However, such test is very difficult to perform on shale due to their very low permeability and may require specialized equipment such as those developed by Belmokhtar et al. [5]. The aim of this paper is to demonstrate relatively simple experimental procedures based on triaxial and oedometer tests in determining the poroelastic properties of a shale. Oedometer and triaxial consolidation tests were carried out on a North Sea reservoir overburden shale. The Biot coefficient α and the drained bulk modulus K are determined by interpreting the experimentally obtained test data using simple methods presented in this paper. The Biot coefficient α values from the oedometer and triaxial tests are compared. The Skempton's coefficient B-value of triaxial samples was also experimentally measured prior to the triaxial consolidation tests and compared with theoretical equations.

2 Overview of poroelasticity theory

The formulation of Biot's poroelasticity theory is provided here for ease of later analysis and discussions. The poroelastic constitutive equations for a fluid-filled porous medium are formulated based upon: (1) assumed linear relationship between the stresses and pore pressure (σ_{ij}, u), and the solid and fluid strains (ε_{ij}, ζ), where σ_{ij} and ε_{ij} are the stress and strain tensors, respectively , u denotes the pore pressure, and ζ is the change in fluid volume per unit volume of the porous medium; and (2) the assumption of zero energy dissipation during a closed loading cycle, i.e., the reversibility of the deformation process.

The linear constitutive equations for a fluid-filled porous material can be obtained by considering the scalar quantities u and ζ in the classic poroelastic stress and strain equations [23]:

$$\varepsilon_{ij} = \frac{\sigma_{ij}}{2G} - \left(\frac{1}{6G} - \frac{1}{9K} \right) \delta_{ij} \sigma_{kk} - \frac{1}{3H'} \delta_{ij} u \qquad (2a)$$

$$\zeta = \frac{\sigma_{kk}}{3H'} - \frac{u}{R'} \qquad (2b)$$

where G and K are the drained shear and bulk moduli of the material, H' and R' characterize the coupling of the stress and strain between the porous material and the fluid. Note that in this study, compressive stresses and strains are positive, and positive ζ indicates a loss of fluid from the porous medium.

The poroelastic constitutive equations Eqs. (2a) and (2b) can be separated into a deviatoric response:

$$e_{ij} = \frac{s_{ij}}{2G} \qquad (3)$$

and a volumetric response:

$$\varepsilon_{\text{vol}} = \frac{\sigma_{\text{m}}}{K} - \frac{u}{H'} \tag{4a}$$

$$\zeta = \frac{\sigma_{\text{m}}}{H'} - \frac{u}{R'} \tag{4b}$$

where $s_{ij} = (\sigma_{ij} - \delta_{ij}\sigma_{\text{m}})$ is the deviatoric stress; e_{ij} is the deviatoric strain; $\sigma_{\text{m}} = \sigma_{kk}/3$ is the mean stress; and $\varepsilon_{\text{vol}} = \varepsilon_{kk}$ is the volumetric strain. Note that the deviatoric response is fully uncoupled from the volumetric response because of the elasticity function (Eq. 2) used herein, and from the fluid response because fluids have no shear stiffness.

Biot [8] proposed the relations between H', R' and α, B and K:

$$\alpha = \frac{K}{H'} \tag{5a}$$

$$B = \frac{R'}{H'} \tag{5b}$$

The poroelastic constitutive equations for the volumetric response can therefore be alternatively expressed as:

$$\varepsilon_{\text{vol}} = \frac{1}{K}(\sigma_{\text{m}} - u\alpha) \tag{6a}$$

$$\zeta = \frac{\alpha}{K}\left(\sigma_{\text{m}} - \frac{u}{B}\right) \tag{6b}$$

where α is Biot poroelastic coefficient and B is the Skempton's coefficient. Note that Eqs. (6a) and (6b) constitute a fully coupled sets of equations and must be strictly solved simultaneously for the unknown variables. Uncoupling of the two equations is only possible under certain prescribed boundary conditions.

3 Test sample material

The samples used in this study were taken from shale core materials which were drilled from the Sele and Lista formations at depth of 2422.5–2445.5 m of the Rogaland group in Well 2/8A-1A in the Valhall Field, Norwegian North Sea. X-Ray Diffraction (XRD) analyses were carried out by the Institute of Geology and Rock Mechanics at the Norwegian University of Science and Technology. Table 1 shows the complete results of the XRD analysis. Also shown in Table 1 are the bulk modulus of corresponding pure mineral components obtained from the literature.

A total of four oedometer tests and six triaxial consolidation tests (four of them were selected and used in the following analysis) were carried out on the test sample at the Norwegian Geotechnical Institute [7]. Specimens for Oedometer tests 1–4 were taken from 3.81 cm (1.5″) plugs at depths of 2445.17–2445.22 m. Specimens for triaxial consolidation tests were taken from seal peel C#2 at depth of 2437.73 m. The materials were stored under high humidity conditions prior to testing. The samples for triaxial tests were drilled from the seal peels using a specially designed drilling equipment to achieve the most consistent samples. The triaxial test samples were held fixed within a special frame during the drilling procedure. An industrial grinder with parallelism of better than 0.01 mm over a length of 300 mm was used to grind both end surfaces of samples. The samples for oedometer tests were obtained by trimming thin slices of shale with the use of a diamond saw. Both end surfaces of the oedometer samples were grinded as for the triaxial samples.

The triaxial samples had approximately 25 mm in diameter. The first two oedometer tests used about 50 mm diameter samples and the other two used about 35.6 mm diameter samples. The porosity, void ratio and saturation were measured for all the samples. Porosity was measured after the test based on the weight of the dried sample grains and the volume of the sample. The obtained porosity and void ratio by considering the effects of micro-fractures vary from 23.87 to 35.93% and 0.31 to 0.56, respectively. The initial degree of saturation ranged from 63.86 to 77.46%. The detailed information of samples for triaxial tests and oedometer tests are given in Tables 2 and 3, respectively.

For triaxial tests, side filter strips were installed at four circumferentially equidistant locations in the triaxial samples to help equilibrate pore pressure distribution in the sample. The filters are high strength polymer strips which can retain their shape and permeability even under high confining pressures. The samples were placed on pedestals and sprayed with a liquid rubber which serves as the confining membrane. Prior to spraying the membrane, four metal pins were glued to the vertical sides of sample (see Fig. 1). These pins protrude through the membrane and serve as contacts for measuring vertical strain. Two of the pins are located diametrically with respect to each other at the lower third point of the specimen height; the other two are located in the same way but at the upper third point and rotated 90° from the first two pins. The use of the target pins allows for accurate measurement of the vertical strain over a sufficient segment of the sample height. In the triaxial drained tests, the fluid volume change ΔV_w was also measured by collecting the fluid flowing out of the sample.

The oedometer was made of high-grade stainless steel with a Young's modulus of 200 GPa. At a maximum effective vertical stress of 25 MPa, the lateral pressure is 12.5 MPa assuming a K_0 value of 0.5. The maximum circumferential strain in the oedometer is only $6.25 \times 10^{-3}\%$ which is sufficiently small to produce oedometric conditions during the tests. Moreover, the poroelasticity determinations were made at low stresses resulting in even smaller oedometer cell compliance.

Table 1 XRD data of shale and bulk modulus of pure mineral components

XRD analysis	Content	Bulk modulus (GPa)	References
Quartz	0.4	35.9–39, with the average value of 37.5	Bass [4], Zinszner and Pellerin [61] and Petrowiki [41]
Smectite	0.4	25–34.8, with the average value of 28	Bass [4], Zinszner and Pellerin [61], Gutierrez et al. [28], Mondol and Nazmul [38] and Wang et al. [58]
NaCl	0.08	24–24.4, with the average value of 24.4	Hofmeister [34], Alkammash [1] and Roylance [46]
Pyritte	0.09	136–147.6, with the average value of 143.6	Bass [4] and Petrowiki [41]
Mica	0.02	49–58, with the average value of 54.2	Smyth et al. [50], Hazen and Finger [31], Catti et al. [15], Comodi and Zanazzi [20] and Pavese et al. [40]
Calcite	0.01	64.5–81.9, with the average value of 71.6	Bass [4], Zinszner and Pellerin [61] and Petrowiki [41]

Table 2 Data on triaxial specimens

Test no.	Depth (m)	Porosity, ϕ (%)	Void ratio, e	Saturation (%)	Size (mm)
N3	2437.73	33.18	0.50	72.1	24.81Φ × 55.77
N4	2437.73	33.72	0.51	68.6	24.98Φ × 55.81
N5	2437.73	33.88	0.51	68.6	24.90Φ × 56.30
N6	2437.73	33.60	0.56	67.4	24.86Φ × 56.64

Table 3 Data on oedometer specimens

Test no.	Depth (m)	Porosity, ϕ (%)	Void ratio, e	Saturation (%)	Size (mm)
1	2445.17	23.87	0.31	63.86	50.45Φ × 19.92
2	2445.20	25.62	0.34	64.74	50.42Φ × 19.09
3	2445.22	28.48	0.40	77.46	35.64Φ × 14.66
4	2445.22	28.68	0.40	76.71	35.66Φ × 14.48

The type of pore fluid plays an important role in maintaining the original characteristics of shale in situ. Many shales particularly those having high smectite mineral composition will swell upon introduction of a fluid with salt content different to original content into the shale sample [19]. It needs to keep the same pore fluid within the sample, or at least know the composition of the original pore fluid of the sample in situ and later re-saturate the samples using the same fluid to avoid shale swelling. Pore fluid was collected by placing core samples in a core holder and forcing pressurized air through it. There is a wide range of tests to analyze the chemical composition and physical indicators of pore fluids, however, the most important is salt content as this can directly affect the swelling potential of shale. The salinity of the shale sample was using salinity meter that passes electric current between two electrodes through the pore fluid and measuring the fluid conductivity which can then be correlated to salt content. The test result provided a value of 98.5 g/l NaCl. The samples after being placed in the triaxial and oedometer chambers were re-saturated using the fluid having the same composition as in situ (salt water with 98.5 g/l NaCl) to avoid swelling of the sample. Back-pressures of 15–20 MPa and 1 MPa were applied for the triaxial and oedometer consolidation tests, respectively, after introducing salt water into the specimens. The saturation of the samples will be evaluated and discussed in Sect. 6.
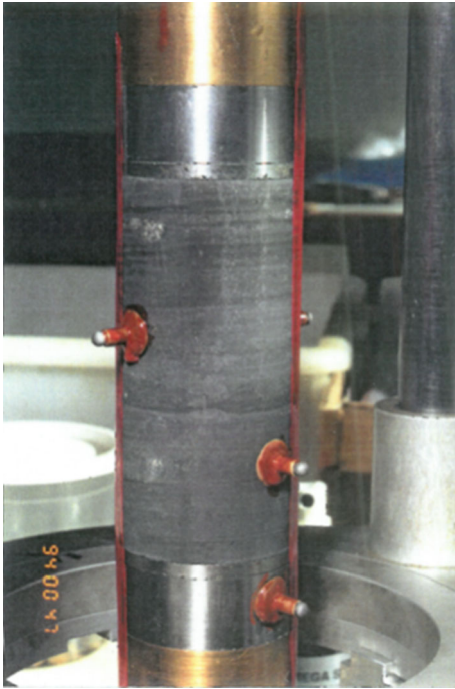
Fig. 1 Sample used in triaxial tests

4 Biot coefficient α and bulk modulus K

The oedometer and triaxial consolidation tests were conducted under drained conditions and hence, the pore pressure which might be generated during the tests were dissipated, i.e., $u = 0$. Equations (6a) and (6b) now become:

$$\varepsilon_{\mathrm{vol}} = \frac{\sigma_{\mathrm{m}}}{K} \tag{7a}$$

$$\zeta = \frac{\alpha}{K} \sigma_{\mathrm{m}} \tag{7b}$$

The Biot coefficient α can be determined by the following equation [57]:

$$\alpha = 1 - \frac{K}{K_{\mathrm{s}}} \tag{8}$$

where K is the drained bulk modulus of the porous medium and K_{s} denotes the bulk modulus of the solid grains of the porous medium.

Note that fully drained conditions are not required in the proposed method. As shown analytically below, achieving drained conditions in shales can take a very long time, making the determination of the poroelastic parameters very expensive. The proposed method should work as well in undrained conditions if the pore pressure in the sample is measured. For undrained conditions, the poroelastic parameters can be determined from Eqs. (6a) and (6b) at any desired stage of loading if the pore pressure is measured during the test. It is well known that achieving uniform pore pressure is easier than obtaining full drainage even in very low-permeability rocks. Moreover, if the pore in the sample is deemed non-uniform, it is possible to derive an analytical solution for the pore distribution in the sample and arrive at an average pore pressure. This was done in Gutierrez et al. [28] where it is also shown that the use of average pore pressure in the sample is enough to provide reliable values for the poroelasticity parameters.

It only happened that the test results used below to validate the proposed procedures were for drained loading. Again, fully drained condition is not a requirement. The oedometer samples used in the validation were only about 1 cm thick, which makes it very easy to achieve drained conditions. For the triaxial tests, the samples are wrapped in vertical strips of filter paper to promote radial drainage which is a lot faster than vertical drainage due to the much higher permeability of shales along the bedding plane compared to the vertical permeability. Full drainage in both types of tests was checked using Taylor's square root of time method.

4.1 Length of time required for unjacketed compression testing

Usually, unjacketed compression test is required to determine the bulk modulus of the solid grains K_{s}. However, it is difficult to conduct this test on shale as a long time will be required for the pore pressure in the sample to reach equilibrium with that applied at the boundary due to the low permeability of shales. Furthermore, special test equipment and setup are needed to carry out the unjacketed compression test. To date, there appears to be no reported studies with regards to the unjacketed tests on shales, except for Belmokhtar et al. [5] in which the tested COx claystone has a relatively high permeability (in the order of 10^{-20} m^2) and a specially designed compression cell was used.

The lowest permeability of shales can be down to 10^{-23} m^2 [11, 17]. The shortest flow path in the cylindrical sample is along the radial direction of the cylinder. The time required for the pore water to reach fluid pressures equal to the pore fluid pressure p_0 applied at the boundary of the cylinder can be formulated as a radially symmetric problem of the pressure development in a circular porous medium, which can be simply illustrated by the diffusion equation [48]:

$$D^2 \left(\frac{\partial^2 p}{\partial r^2} + \frac{1}{r} \frac{\partial p}{\partial r} \right) = \frac{\partial p}{\partial t} \tag{9}$$

where

$$D^2 = \frac{K_p}{\eta_f(nC_f + C_D)} \tag{10}$$

and K_p is the permeability of shales, η_f is the dynamic viscosity of the fluid, n is the porosity, and C_f and C_D are the compressibilities of the fluid and the skeleton, respectively. At the time of $t = 0$, a pressure pulse is applied at the boundary of the circular sample and the pore pressure within the circular domain is zero. The boundary and initial conditions which control the pore pressure diffusion into the circular domain of radius a are expressed by:

$$p(a,t) = p_0 H(t); \forall_t \geq 0 \tag{11}$$

$$p(r,0) = 0; 0 \leq r \leq a \tag{12}$$

where $H(t)$ is the Heaviside step function of time. The analytical solution to the pressure evolvement in the circular porous region can be expressed as [47]:

$$p(r,0) = p_0 \left(1 - 2 \sum_{n=1,2}^{\infty} \frac{\exp(-k_n^2 D^2 t) J_0(k_n r)}{[k_n a J_1(k_n a)]} \right) \tag{13}$$

where J_0 and J_1 are zeroth-order and first-order Bessel functions of the first kind. k_n are the roots of the characteristic equation:

$$J_0(k_n a) = 0 \tag{14}$$

The pore fluid pressure development at the center of the circular sample can be computed by the simplified form of Eq. (13):

$$p(0,t) = p_0 \left(1 - 2 \sum_{n=1,2}^{\infty} \frac{\exp(-k_n^2 D^2 t)}{[k_n a J_1(k_n a)]} \right) \tag{15}$$

Equation (15) is used to compute the time-dependent pressure development at the center of the circular sample by considering the physical properties of the low-permeability shale and the experimental configuration which are listed in Table 4.

In Eq. (15), D^2 can be computed using Eq. (10) and the parameters shown in Table 4. The parameter k_n, the roots of the characteristic equation Eq. (14), is solved using the Bessel Zero Solver which can be downloaded from the Mathworks website [13]. $J_1(k_n a)$ can be computed using the Bessel function of first kind, Besselj, which is implemented in MATLAB R2019b. Time t (in s) is the parameter to be determined by trial and error.

For the experimental configuration used in this study as given in Table 4, the time required for the pore pressure at the center of the circular sample to reach 99% of the boundary pressure is approximately 243 days. The required time is closely associated with the permeability of the porous medium. The increase of the permeability of K_p to 10^{-22} m^2 will decrease the time requirement to 25 days,

Table 4 Experimental configuration and physical properties of shale

Parameters	Value
Permeability K_p[a]	10^{-23} m^2
Skeleton compressibility C_D[b]	3.1×10^{-11} (Pa)$^{-1}$
Fluid compressibility C_f[c]	4.3×10^{-10} (Pa)$^{-1}$
Porosity n[d]	0.34
Sample radius a[e]	0.025 m
Dynamic viscosity of the fluid η_f[f]	0.002 Pa s
Time t	To be determined, s

[a]The permeability can be as low as 10^{-23}m^2 which was also confirmed by [11, 39]

[b]The inverse of the compressibility is called the bulk modulus and hence, the skeleton compressibility is equal to $1/K_s$ which refers to the bulk modulus of the solid grains of the porous medium. According to Sect. 4.1, the lower bound of K_s is 32 GPa and hence 1/32 GPa = 3.1×10^{-11}(Pa)$^{-1}$

[c]Fluid compressibility is determined as inverse of the bulk modulus of seawater which is 2.34 GPa [2, 18]. Hence the used compressibility is 1/2.34 GPa = 4.3×10^{-10}(Pa)$^{-1}$

[d]Porosity of the shale samples was measured based on the total volume of the sample and the volume of the solids. The latter was obtained by crushing the sample after each test and placing the crushed materials in a pycnometer. To check the volume of the solids, the weight of the dried crushed sample was also determined and converted to volume of solids using the specific gravity of the minerals composing the solids

[e]The radius of the samples was measured with a pi-tape micrometer, and the largest value of 0.025 m was used (Table 2)

[f]Fluid viscosity is taken from the dynamic viscosity of seawater as 0.002 Pa s [12, 16]

which is still significant. The effective fluid compressibility of shales would increase when the pores in the samples contain undissolved air, which will lead to the increase of the time required to reach saturation. Furthermore, complete saturation of all the accessible pore spaces cannot be guaranteed when laboratory techniques are deployed to fully saturate the low-permeability rocks. On the other hand, shales in the field can be saturated when subjected to geological time, stress sates and fluid supply conditions.

4.2 Alternative method to determine the grain bulk stiffness

Due to reason discussed above, unjacketed tests were not conducted in this study and instead alternative theoretical procedures are used to estimate K_s. To do it precisely one must consider [3]: (1) the individual bulk modulus of the constituents; (2) the volume fractions of the constituents; (3) geometric details of how the various constituents are arranged. The first two information of the shale in this study are already obtained and shown in Table 1 whereas

the geometric details are difficult to measure. Without the knowledge of the details of geometry, the best one can do is estimate the upper and lower bounds of the bulk modulus. The bound estimation is a powerful and robust tool which provides rigorous upper and lower limits on the bulk modulus. Several researchers have developed theoretical estimates to determine the elasticity properties of multi-phasic materials [30, 32, 33, 44, 56]. The Voigt–Reuss bounds are the simplest bounds which provide upper and lower limits for the effective elasticity properties of rocks, whereas Hashin and Shtrikman [30] proposed the narrowest possible bounds. To make the predictions more reliable, Voigt and Reuss estimates are used to determine the upper and lower bounds on the bulk modulus of the solid grains of shale K_s.

The upper bound estimate is computed by the Voigt average:

$$K_s^U = \sum_{i=1}^{n} X_i K_{m,i} \tag{16}$$

The lower bound estimate is computed by the Reuss average:

$$K_s^L = \left(\sum_{i=1}^{n} \frac{X_i}{K_{m,i}} \right)^{-1} \tag{17}$$

where K_s^U is the upper bound of the effective bulk modulus; K_s^L is the lower bound of the effective bulk modulus, X_i and $K_{m,i}$ are the content and the bulk modulus of each mineral component. The mineral composition of the tested shale is shown in Table 1. It can be seen that the bulk modulus of the minerals is a range. The minimum values of the bulk modulus of the minerals are implemented in Eqs. (16) and (17), leading to K_s in range from 32.0 to 40.0 GPa; the implementation of maximum values of the bulk modulus results in K_s ranging from 38.0 to 46.0 GPa. Hence, the determined K_s of the shale sample in this study ranges from 32.0 to 46.0 GPa.

4.3 Determination of the poroelastic parameters from triaxial consolidation tests

The vertical strain ε_v, effective vertical and horizontal stresses σ_v' and σ_h', and the fluid volume change ΔV_w, were measured during the triaxial tests. The triaxial test No. 3 was isotropically consolidated to a mean effective stress of 3 MPa. To mimic the actual stress condition in the field, the triaxial tests 4–6 were all anisotropically consolidated to an effective major principal stress of $\sigma_v' = 4$ MPa and to an effective minor principal stress of $\sigma_h' = 2$ MPa.

The fluid content variation ζ can be computed by:

$$\zeta = \frac{\Delta V_w}{V} \tag{18}$$

where V denotes the volume of the porous medium.

Combining Eqs. (7b) and (8) leads to:

$$\zeta = \left(\frac{1}{K} - \frac{1}{K_s} \right) \sigma_m \tag{19}$$

The mean stress σ_m in Eq. (19) is equal to the effective mean stress σ_m' as the pore pressure $u = 0$ due to the drained condition. Hence, Eq. (19) becomes:

$$\zeta = \left(\frac{1}{K} - \frac{1}{K_s} \right) \sigma_m' \tag{20}$$

The relationships between ζ and σ_m' of the four triaxial consolidation tests are shown in Fig. 2. The slope of the σ_m'–ζ curves shown in Fig. 2 is equal to $(1/K - 1/K_s)$ and the bulk modulus K can be computed with the K_s range of 32–46 GPa. The Biot coefficient α can be computed using Eq. (8). The computed bulk modulus K and the Biot coefficient α are listed in Table 5. It is observed that the obtained Biot coefficient α are similar for all the four samples, varying in the range of 0.95–0.99 while the computed bulk modulus K has a relatively large range varying from 0.32 to 1.61 GPa.

It is worth noting that the isotropically consolidated sample No. 3 and the anisotropically consolidated samples No. 4–6 produce consistent values for the bulk modulus K and the Biot coefficient α.

4.4 Determination of the poroelastic parameters from oedometer consolidation tests

The vertical strain ε_v and the effective vertical stress σ_v' were measured for the oedometer tests. The effective horizontal stress and the water content change were not monitored during the oedometer tests. The fluid content variation ζ and the effective mean stress σ_m' are not available and the method used in the determination of the K and α for triaxial tests is not applicable in the oedometer test.

The laboratory measurements provide the relationships between the effective vertical stress σ_v' and the vertical strain ε_v for the four oedometer tests, which are shown in Fig. 3. The constrained modulus M can be determined according to the curves in the figure. Table 6 lists the obtained constrained modulus M for the four oedometer tests.

The bulk modulus K can be expressed as a function of the constrained modulus M and the Poisson's ratio v for linear elastic materials:
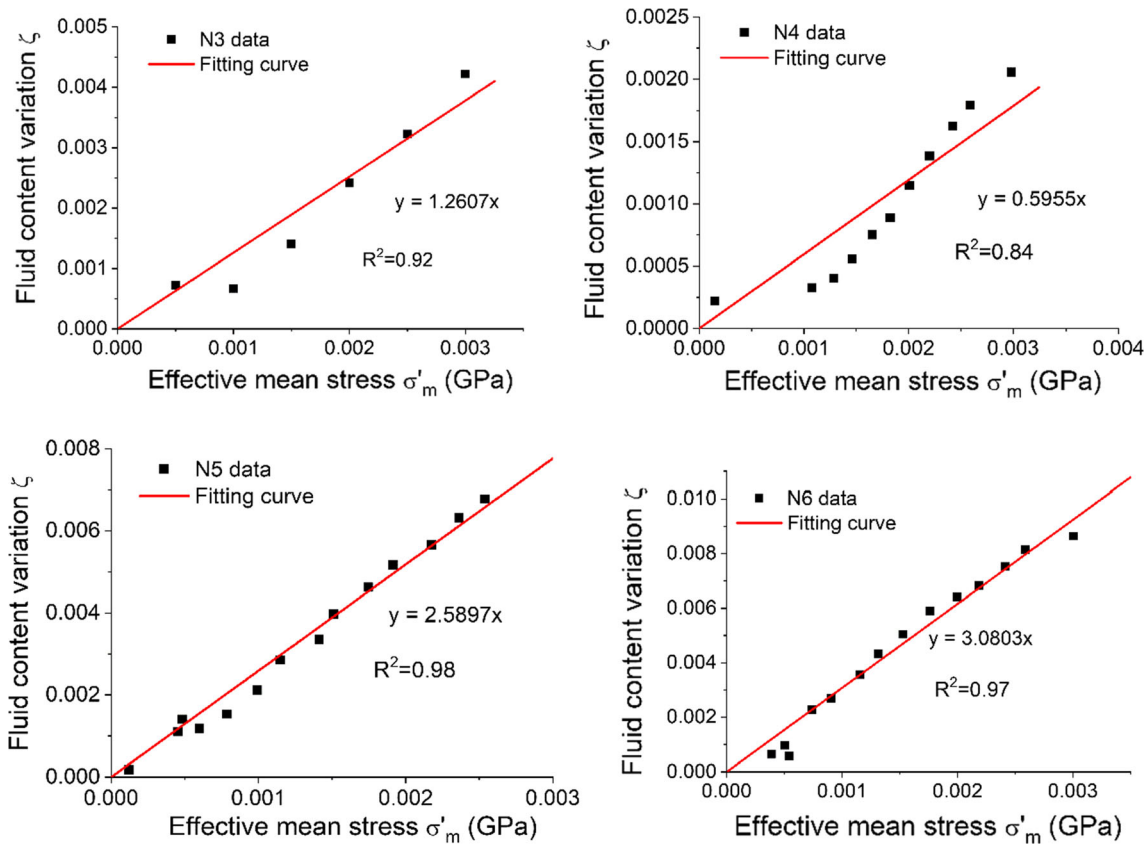
Fig. 2 The relations between ζ and σ'_m for the 4 triaxial consolidation

Table 5 The bulk modulus K and Biot coefficient α computed from triaxial tests

Test no.	$\frac{1}{K} - \frac{1}{K_s}$ 1/GPa	Lower bound K_s^L, 32 GPa		Upper bound K_s^U, 46 GPa	
		Bulk modulus K, GPa	Biot coefficient, α	Bulk modulus K, GPa	Biot coefficient, α
N3	1.26	0.77	0.98	0.78	0.98
N4	0.60	1.58	0.95	1.61	0.97
N5	2.59	0.38	0.99	0.38	0.99
N6	3.08	0.32	0.99	0.32	0.99

$$K = \frac{M(1+v)}{3(1-v)} \tag{21}$$

According to the studies of Sone and Zoback [51], Islam and Skalle [35], and Eshkalak et al. [24], the Poisson's ratio of shale ranges from 0.1 to 0.5. K can be estimated using Eq. (21) for v between 0.1 and 0.5. Figure 4a shows how the estimates of K varies for the four oedometer tests and Table 7 lists the detailed information. The Biot coefficient α can then be computed using Eq. (8) based on the estimates of K. Figure 4b shows the range of the Biot coefficient α of the four oedometer tests and Table 8 gives the detailed information.

It can be seen that the obtained K value for the oedometer tests ranges from 0.17 to 2.00 GPa and the Biot coefficient α ranges from 0.95 to 0.99 for v of 0.1 to 0.5. The oedometer K value of 0.17–2.00 GPa has a wider range than the K value of 0.32–1.61 GPa computed from the triaxial tests. The oedometer α value of 0.95–0.99 is to the same to the α value of 0.95–0.99 from the triaxial tests.

Berre et al. [7] conducted triaxial shear tests on the samples after the triaxial consolidation stage. The Young's modulus and the Poisson's ratio were determined at the 50% of the peak stress in the stress–strain curves and they are denoted as E_{50} and v_{50}. The obtained Poisson's ratio v_{50} ranges from 0.34 to 0.49. The K value computed using v_{50}
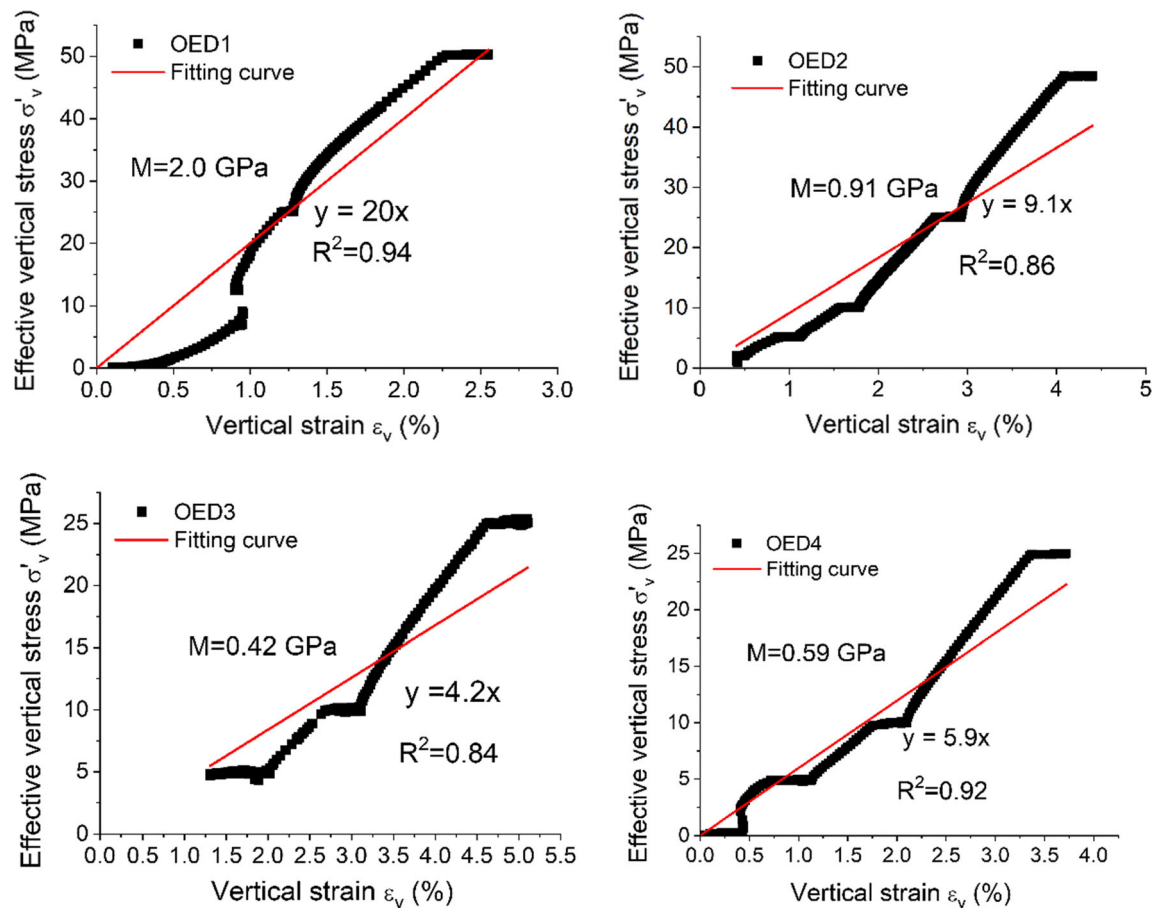
Fig. 3 The relationships between the effective vertical stress σ'_v and the vertical strain ε_v for oedometer tests

Table 6 The constrained modulus M determined from oedometer tests

Test no.	Constrained modulus M, GPa
OED1	2.00
OED2	0.91
OED3	0.42
OED4	0.59

of 0.34–0.49 ranges from 0.41 to 2.2 GPa, which agrees well with the triaxial K value of 0.32–1.61 GPa. The obtained Biot coefficient α using v_{50} of 0.34–0.49 ranges from 0.95 to 0.98, which shows a good agreement with the triaxial α value of 0.95–0.99. The good agreement between the triaxial and oedometer consolidation tests in terms of the computed Biot coefficient α and bulk modulus K indicates the reliability of the obtained data and the capability of the presented methods in determining reliable α and K values, which is higher than the Biot's coefficient α of 0.3–0.6 which was obtained under the effective mean stress of 20–50 MPa by Gutierrez et al. [28] for the Mancos

shale. The high Biot coefficient α can be attributed to the low effective mean stress (2–3 MPa) used in this study and the significantly much higher stiffness of Mancos shale.

5 Skempton's *B*-value

Skempton [49] introduced the coefficient B which is defined as the ratio of the pore pressure change to the change of the confining pressure in undrained condition. The B-value for porous medium with the porosity ϕ can be computed by:

$$B = \frac{1}{1 + \frac{K}{K_f}} \quad (22)$$

where K is the drained bulk modulus of the material; and K_f is the bulk modulus of the pore fluid.

For soils, the bulk modulus K is on the order of MPa and is negligible when compared to the fluid bulk modulus K_f which is on the order of GPa [37]. Hence, B is approximately equal to 1.0 for soils. However, the bulk modulus K of rock, which is on the order of GPa is comparable to the
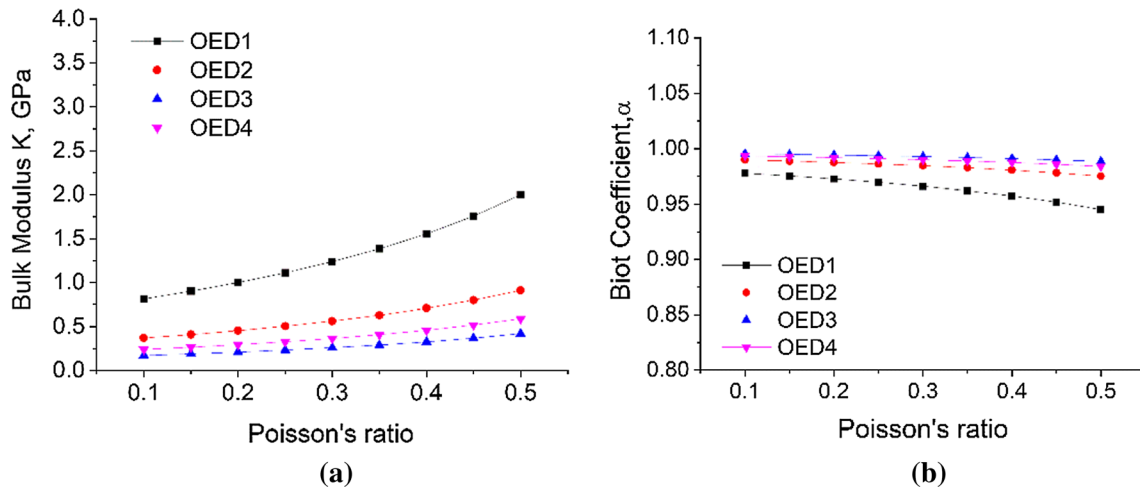
Fig. 4 **a** Bulk modulus K versus Poisson's ratio; **b** Biot coefficient α versus Poisson's ratio

Table 7 The range of bulk modulus K for the four oedometer tests

Poisson's ratio, v	OED1 K, GPa	OED2 K, GPa	OED3 K, GPa	OED4 K, GPa
0.1	0.81	0.37	0.17	0.24
0.15	0.90	0.41	0.19	0.27
0.2	1.00	0.46	0.21	0.30
0.25	1.11	0.51	0.23	0.33
0.3	1.24	0.56	0.26	0.37
0.35	1.38	0.63	0.29	0.41
0.4	1.56	0.71	0.33	0.46
0.45	1.76	0.80	0.37	0.52
0.5	2.00	0.91	0.42	0.59

Table 8 The range of Biot coefficient α for the four oedometer tests

Poisson's ratio, v	OED1 α	OED2 α	OED3 α	OED4 α
0.1	0.98	0.99	0.99	0.99
0.15	0.98	0.99	0.99	0.99
0.2	0.97	0.99	0.99	0.99
0.25	0.97	0.99	0.99	0.99
0.3	0.97	0.98	0.99	0.99
0.35	0.96	0.98	0.99	0.99
0.4	0.96	0.98	0.99	0.99
0.45	0.95	0.98	0.99	0.99
0.5	0.95	0.98	0.99	0.98

fluid bulk modulus K_{f}, and as a result B can be less than 1.0 for rock.

Equation (22) was extended to include the influence of the bulk modulus of the solid grains K_{s} [7, 10, 23]:

$$B = \frac{1}{1 + \frac{K}{\alpha}\left(\frac{1}{K_{\mathrm{f}}} - \frac{1}{K_{\mathrm{s}}}\right)} \tag{23}$$

Skempton's coefficient B was determined for all the triaxial test samples at 20 min after the start of B-value determination. The saltwater bulk modulus K_f of 2.34 GPa was used in the calculation of B. The experimentally obtained B ranges from 0.80 to 0.85 and are listed in Table 9. B-values were also predicted for the triaxial test samples using Eqs. (22) and (23) and the lower and upper bonds of K_{s}, which are shown in Table 9 for comparison. B-values calculated by Eq. (22) using the lower and upper bounds of K_{s} are the same for each sample whereas B-values calculated by Eq. (23) using the lower bound is slightly larger than those from the upper bound. The data given in Table 9 are also plotted in Fig. 5 where the B-values determined from Eqs. (22) and (23) are, on the average, only about 10% higher than the experimentally determined B-values based on linear regression of the data.

Equations (22) and (23) predict almost the same B which range from 0.81 to 0.96. The computed B-values are higher than the experimentally obtained values, with the difference most prominent at small bulk modulus K. The computed B-values for sample No. 4 using K value of 1.58 GPa and the lower bound of K_{s}, and using K value of 1.61 GPa and the upper bound of K_{s}, respectively, agree well with the experimentally obtained B-values. For the rest samples, the computed B-values are larger than the experimentally measured ones due to the small K value. Furthermore, the dominant value for the bulk modulus K of overburden shale can be large value (for instance, between 1.58 and 1.61 GPa for N4 sample).

Table 9 Comparison of experimentally and theoretically obtained B-values using the lower and upper bounds of K_s

| Test no.	Porosity, ϕ, %	Experimental B-value	Lower bound K_s^L, 32 GPa				Upper bound K_s^U, 46 GPa			
			Biot coefficient α	Bulk Modulus K, GPa	B-value by Eq. (22)	B-value by Eq. (23)	Biot coefficient α	Bulk Modulus K, GPa	B-value by Eq. (22)	B-value by Eq. (23)
N3	33.18	0.80	0.98	0.77	0.90	0.91	0.98	0.78	0.90	0.90
N4	33.72	0.81	0.95	1.58	0.81	0.82	0.96	1.61	0.81	0.81
N5	33.88	0.81	0.99	0.38	0.95	0.95	0.99	0.38	0.95	0.95
N6	33.60	0.85	0.99	0.32	0.96	0.96	0.99	0.32	0.96	0.96
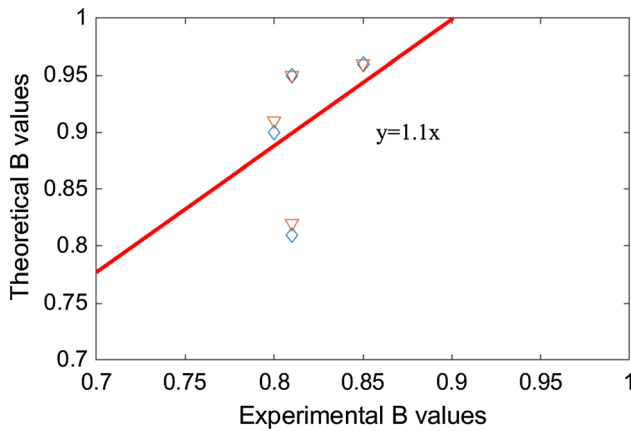
Fig. 5 Comparisons of B-values determined from Eqs. (22) and (23) with experimentally determined B-values

6 Evaluation of the saturation of the samples

The saturation of samples was evaluated by the B-values. When samples are not fully saturated, the pores of samples are occupied by the fluid and air bubbles. The entrapped air reduces the bulk modulus of the fluid. K_f in Eqs. (22) and (23) needs to be replaced by the bulk modulus K_{mix} of the fluid–gas mixture. K_{mix} can be calculated by the following equation [36]:

$$\frac{1}{K_{mix}} = \frac{s_f}{K_f} + \frac{1 - s_f}{K_{gas}} \tag{24}$$

where s_f is the saturation; K_{gas} is the bulk modulus of air bubble. If the temperature remains unchanged during the triaxial consolidation tests, i.e., the isothermal process, the bulk modulus of the gas is equal to its pressure which is considered to be equal to the back pressure applied on the samples. The backpressures of 15–20 MPa are used in the triaxial tests and hence $K_{gas} = 15 - 20$ MPa. Only Eq. (22) is used in this evaluation as Eqs. (22) and (23) produce similar B-values. The computed B-values based on saturation $s_f = 0.98$ and 0.99 and $K_{gas} = 15$ and 20 MPa are shown in Table 10. Higher degree of saturation leads to

larger B-values and larger backpressure results in larger B-values. Hence, $K_{gas} = 20$ MPa and $s_f = 0.99$ result in the largest B-values of the four cases in Table 10. Figure 6 shows the comparisons between experimental B-values and the computed ones, as well as their linear regression. The B-values for $K_{gas} = 20$ MPa and $s_f = 0.99$ are less than the experimental B-values. In this sense, saturation s_f of the samples in this study can be considered larger than 0.99.

7 Discussion on the validity of the proposed procedures on determining the poroelastic properties

The proposed procedure on determining the poroelastic properties includes poroelastic equations Eqs. (6a) and (6b) and regular oedometer and triaxial consolidation tests. The procedure proposed in this paper should be valid in terms of theoretical background and laboratory tests. The following will demonstrate the validity of the poroelastic theories used in this study. Equation (6b) is selected because the experiments conducted in this study monitored the volume change of fluid flowing in or out the samples. Equation (6a) and Eq. (6b) are comparable and any one of the two equations can be used to predict the poroelastic properties. The theory is valid once any one of Eqs. (6a) and (6b) is proved valid.

The following will demonstrate the validity of the theories using the test results of Belmokhtar et al. [5]. Equation (6a) will be evaluated as Belmokhtar et al. [5] measured the volumetric strain using LVDTs. The incremental form of Eq. (6a) is expressed as:

$$d\varepsilon_{vol} = \frac{1}{K}(d\sigma_m - \alpha du) \tag{25}$$

Belmokhtar et al. [5] investigated the poroelastic properties of the COx claystone by carrying out an unjacketed compression test in which pore pressure and confining stress are simultaneously changed, an undrained test in which pore pressure is changed under constant total stress,

Table 10 Comparison of experimentally and theoretically obtained B-values based on the saturation

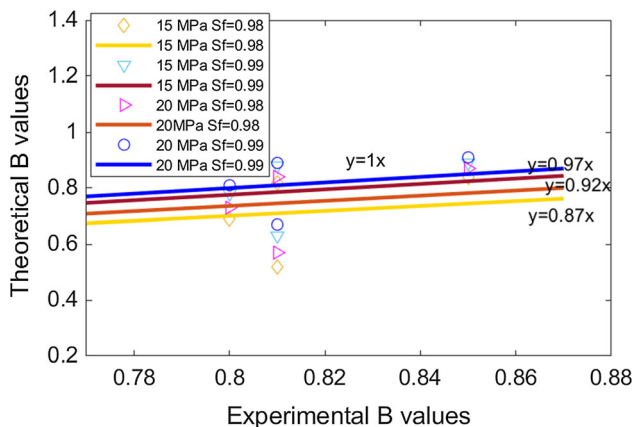| Test no.	Experimental B-value	Backpressure 15 MPa		Backpressure 20 MPa	
		$s_f = 0.98$	$s_f = 0.99$	$s_f = 0.98$	$s_f = 0.99$
N3	0.8	0.69	0.78	0.73	0.81
N4	0.81	0.52	0.63	0.57	0.67
N5	0.81	0.82	0.88	0.84	0.89
N6	0.85	0.84	0.89	0.87	0.91

Fig. 6 Comparisons of experimental and computed B-values by Eq. (22)

and a drained compression test in which the confining stress under constant pore pressure. The unjacketed test directly gave the bulk modulus of the solid grains of $K_s = 21.73$ GPa. For the undrained test, the total stress is constant and hence $d\sigma_m = 0$. With $\alpha = 1 - K/K_s$, Eq. (25) becomes:

$$d\varepsilon_{vol} = -\left(\frac{1}{K} - \frac{1}{K_s}\right) du \qquad (26)$$
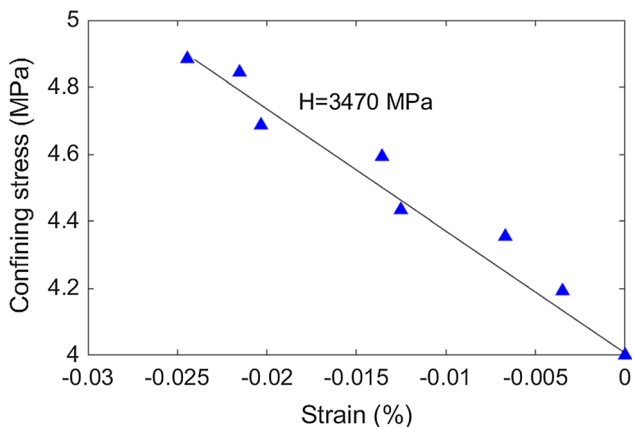

Fig. 7 The curve between confining stress versus volumetric strain of the undrained test from Belmokhtar et al. [5]

Figure 7 shows the relationship between the confining stress and the volumetric strain of the undrained test. From the figure, one has the following equation:

$$\frac{1}{K} - \frac{1}{K_s} = \frac{1}{3470\,\mathrm{MPa}} \qquad (27)$$

The drained bulk modulus K is calculated as 2992 MPa. For the drained compression test of Belmokhtar et al. [5], the drained bulk modulus K can be directly obtained from the curve of the confining stress and the volumetric strain. The slope of the curve is 2985 MPa, which is the value of K according to $d\varepsilon_{vol} = \frac{1}{K}d\sigma_m$. The computed K of 2992 MPa matches well with the K of 2985 MPa experimentally obtained by Belmokhtar et al. [5]. This provides independent confirmation that the theoretical Eqs. (6a) and (6b) are reliable in predicting the poroelastic properties.

8 Conclusions

The determination of the poroelastic parameters usually require specially designated test setups, which many labs do not have access to. Regular oedometer and triaxial consolidation tests were conducted and simple methods were presented in this study to interpret the experimental results. The poroelastic parameters Biot coefficient α and Skempton's coefficient B of a North Sea shale were determined. The Biot coefficient α for the tested shale computed from the oedometer and triaxial tests varied from 0.95 to 0.99. The high Biot coefficient α can be due to the low effective mean stresses used in the tests. The drained bulk modulus K is also computed from the oedometer and triaxial tests. The obtained K value has a range of 0.17–2.00 GPa.

The Skempton's coefficient B was experimentally measured in the triaxial tests. The obtained B-value ranged from 0.8 to 0.85. The theoretically predicted B-value varied from 0.81 to 0.96 which was, on the average, only about 10% higher than the experimental values with the most apparent difference observed at low bulk modulus. Theoretical equations for the Skempton's coefficient B can lead

to more accurate estimates of B when K is between 1.58 and 1.61 GPa. Further validation of the proposed procedures was made using the experimental results of Belmokhtar et al. [5].

The proposed method avoids the need for very time consuming and expensive unjacketed compression testing to determine the bulk modulus of the rock grains, which, in the case of shales, may require specialized equipment that is not necessarily available in routine testing. Also, the proposed procedure does not strictly require fully drained conditions and can be also be used in conjunction with undrained testing with pore pressure measurement. Thus, the proposed method is ideally suited to the routine determination of poroelastic parameters that is practical yet sufficiently accurate.

The good agreement between the triaxial and oedometer consolidation tests in terms of the computed Biot coefficient α and bulk modulus K indicates the reliability of the obtained data and the presented methods in determining reliable α and K values. Additionally, the procedures have been validated by comparison with the results of Belmokhtar et al. [5] using unjacketed compression tests. As with any geomechanical testing, there will be inherent uncertainties and users must exercise judgment in the selection and use of results.

References

1. Alkammash IY (2013) Evaluation of pressure and bulk modulus for alkali halides under high pressure and temperature using different EOS. J Assoc Arab Univ Basic Appl Sci 14(1):38–45
2. Altera A, Bayraktar O, Cetin M (2019) Advanced road materials in highway infrastructure and features. Kastamonu Univ J Eng Sci 5(1):36–42
3. Avseth P, Mukerji T, Mavko GM (2005) Quantitative seismic interpretation: applying rock physics tools to reduce interpretation risk. Cambridge University Press, Cambridge
4. Bass JD (1995) Elasticity of minerals, glasses, and melts. Mineral physics and crystallography: a handbook of physical constants. AGU Ref. Shelf. T. J. Ahrens, Washington, DC
5. Belmokhtar M, Delage P, Ghabezloo S, Tang A-M, Menaceur H, Conil N (2017) Poroelasticity of the Callovo–Oxfordian claystone. Rock Mech Rock Eng 50(4):871–889
6. Berge PA, Wang HF, Bonner BP (1993) Pore pressure buildup coefficient in synthetic and natural sandstones. Int J Rock Mech Min Sci Geomech Abstr 30(7):1135–1141
7. Berre T, Gutierrez M, Høeg K, Nagel N, Kristiansen T (1996) Laboratory testing of an overburden shale. In: Proceedings of 5th North Sea Chalk Symposium, Reims, France, October 7–9, 1996, paper no. IV-2
8. Biot MA (1941) General theory of three-dimensional consolidation. J Appl Phys 12(2):155–164
9. Biot MA, Willis DG (1957) The elastic coefficients of the theory of consolidation. J Appl Mech 24:594–601
10. Bishop AW (1973) The influence of an undrained change in stress on the pore pressure in porous media of low compressibility. Geotechnique 23(3):435–442
11. Brace WF (1980) Permeability of crystalline and argillaceous rocks. Int J Rock Mech Min Sci Geomech Abstr 17(5):241–251
12. Brooks R, Cetin M (2012) Application of construction demolition waste for improving performance of subgrade and subbase layers. Int J Res Rev Appl Sci 12(3):375–381
13. Brooks R, Cetin M (2013) Water susceptible properties of silt loam soil in sub grades in South West Pennsylvania. Int J Mod Eng Res 3(2):599–603
14. Busch A, Alles S, Gensterblum Y, Prinz D, Dewhurst DN, Raven MD, Stanjek H, Krooss BM (2008) Carbon dioxide storage potential of shales. Int J Greenhouse Gas Control 2(3):297–308
15. Catti M, Ferraris G, Hull S, Pavese A (1994) Powder neutron diffraction study of 2M1 muscovite at room pressure and at 2 GPa. Eur J Miner 6:171–178
16. Cetin M (2013a) Pavement design with porous asphalt. Ph.D. thesis, Temple University
17. Cetin M (2015) Consideration of permeable pavement in landscape architecture. J Environ Prot Ecol 16(1):385–392
18. Cetin M Chapter 55: using recycling materials for sustainable landscape planning, environment and ecology at the beginning of 21st century, ST. Kliment Ohridski University Press, pp 783–788
19. Chenevert ME (1970) Shale alteration by water adsorption. J Pet Technol 22:1–141
20. Comodi P, Zanazzi PF (1995) High pressure structural study of muscovite. Phys Chem Miner 22:170–177
21. Coussy O (2004) Poromechanics. Wiley, Hoboken, p 9780470849200
22. Dayal AM (2017) Chapter 1—shale. In: Dayal AM, Mani D (eds) Shale gas. Elsevier, Amsterdam, pp 1–11
23. Detournay E, Cheng AHD (1993) Fundamentals of poroelasticity. In: Hundson JA (ed) Analysis and design methods. Pergamon, Oxford, pp 113–171
24. Eshkalak MO, Mohaghegh SD, Esmaili S (2014) Geomechanical properties of unconventional shale reservoirs. J Pet Eng 2014:10
25. Ferrari A, Laloui L (2013) Advances in the testing of the hydromechanical behaviour of shales. Springer, Berlin, pp 57–68
26. Gutierrez MS, Lewis RW (2002) Coupling of fluid flow and deformation in underground formations. J Eng Mech 128(7):779–787
27. Gutierrez M, Katsuki D, Almrabat A (2012) Effects of CO_2 injection on the seismic velocity of sandstone saturated with saline water. Int J Geosci 3(5A):908–917
28. Gutierrez M, Katsuki D, Tutuncu A (2015) Determination of the continuous stress-dependent permeability, compressibility and poroelasticity of shale. Mar Petrol Geol 68:614–628
29. Han DH, Nur A, Morgan D (1986) Effects of porosity and clay content on wave velocities in sandstones. Geophysics 51(11):2093–2107
30. Hashin Z, Shtrikman S (1963) A variational approach to the elastic behavior of multiphase minerals. J Mech Phys Solids 11:127–140
31. Hazen RM, Finger LW (1978) The crystal structures and compressibilities of layer minerals at high pressure. II. Phlogopite and chlorite. Am Miner 63:293–296
32. Hill R (1963) Elastic properties of reinforced solids: some theoretical principles. J Mech Phys Solids 11:357–372
33. Hill R (1965) A self-consistent mechanics of composite materials. J Mech Phys Solids 13:213–222
34. Hofmeister AM (1991) Calculation of bulk modulus and its pressure derivatives from vibrational frequencies and mode Grüneisen parameters: solids with cubic symmetry or one nearest-neighbor distance. J Geophys Res Solid Earth 96(B10):16181–16203
35. Islam MA, Skalle P (2013) An experimental investigation of shale mechanical properties through drained and undrained test mechanisms. Rock Mech Rock Eng 46(6):1391–1413

36. Kafesaki M, Penciu R, Economou E (2000) Air bubbles in water: a strongly multiple scattering medium for acoustic waves. Phys Rev Lett 84:6050

37. Makhnenko RY, Labuz JF (2013) Saturation of porous rock and measurement of the B . In: 47th U.S. rock mechanics/geomechanics symposium. American Rock Mechanics Association, San Francisco, California, p 6

38. Mondol NH et al (2008) Elastic properties of clay minerals. Leading Edge 27:758–770

39. Neuzil CE (1994) How permeable are clays and shales? Water Resour Res 30(2):145–150

40. Pavese A, Ferraris G, Pischedda V, Mezouar M (1999) Synchrotron powder diffraction study of phengite 3T from the Dora-Maira Massif: P-V-T equation of state and petrological consequences. Phys Chem Miner 26:460–467

41. PetroWiki (2015) Isotropic elastic properties of minerals. https://petrowiki.org/Isotropic_elastic_properties_of_minerals. Accessed 25 Apr 2020

42. Prevost JH (1980) Mechanics of continuous porous media. Int J Eng Sci 18:787–800

43. Prevost JH (1982) Nonlinear transient phenomena in saturated porous media. Comput Method Appl M 20:3–8

44. Reuss A (1929) Berechnung der Fließgrenze von Mischkristallen auf Grund der Plastizitätsbedingung für Einkristalle. J Appl Math Mech 9:49–58

45. Rice JR, Cleary MP (1976) Some basic stress diffusion solutions for fluid saturated elastic porous media with compressible constituents. Rev Geophys Space Phys 14:227–241

46. Roylance D (2000) Atomistic basis of elasticity. Massachusetts Institute of Technology, Cambridge

47. Selvadurai APS (2000) Partial differential equations in mechanics, Vol. 1. Fundamentals, Laplace' equation, the diffusion equation, the wave equation. Springer, Berlin

48. Selvadurai APS (2018) The Biot coefficient for a low permeability heterogeneous limestone. Continuum Mech Therm 31:1–15

49. Skempton AW (1954) The pore-pressure coefficients A and B. Geotechnique 4(4):143–147

50. Smyth JR, Jacobsen SD, Swope RJ, Angel RJ, Arlt T, Domanik K, Holloway JR (2000) Crystal structures and compressibilities of synthetic 2M1 and 3T phengite micas. Eur J Miner 12(5):955–963

51. Sone H, Zoback MD (2013) Mechanical properties of shale-gas reservoir rocks—part 1: static and dynamic elastic properties and anisotropy. Geophysics 78(5):D381–D392

52. Terzaghi K (1923) Die Berechnung der Durchl̈assigkeitsziffer des Tones aus dem Verlauf der hydrodynamische Spannungserscheinungen. Sitzber Akad Wiss Wien Abt IIa 132:125–138

53. Terzaghi K (1925) Erdbaumechanik auf Bodenphysikalicher Grundlage. Franz Deutike, Vienna

54. Tsang CF, Barnichon JD, Birkholzer J, Li XL, Liu HH, Sillen X (2012) Coupled thermo-hydro-mechanical processes in the near field of a high-level radioactive waste repository in clay formations. Int J Rock Mech Min 49:31–44

55. Verruijt A (1969) Elastic storage of aquifers, flow through porous media. Academic Press, New York

56. Voigt W (1928) Lehrbuch der Kristallphysik. Teubner, Leipzig

57. Wang HF (1993) Quasi-static poroelastic parameters in rock and their geophysical applications. Pure Appl Geophys 141(2):269–286

58. Wang Z, Wang H, Cates M (2001) Effective elastic properties of solid clays. Geophysics 66(2):428–440

59. Xue Z, Mito S, Kitamura K, Matsuoka T (2009) Case study: trapping mechanisms at the pilot-scale CO_2 injection site, Nagaoka, Japan. Energy Procedia 1(1):2057–2062

60. Zienkiewicz OC, Chang CT, Bettess P (1980) Drained, undrained, consolidating and dynamic behaviour assumptions in soils. Geotechnique 30:385–395

61. Zinszner B, Pellerin FM (2007) A geoscientist's guide to petrophysics. Editions Technip, Paris